

Adjusted method to calculate an electric wheelchair power cycle: fuel cell implementation example

Dafne Zuleima Morgado Ramirez^{a,b,*}, Lara Rasha^{c,1}, Giulia Barbareschi^{a,b}, Tatsuto Suzuki^d, Irving Caplan^e, Iain McKinnon^b, Dan J.L. Brett^c, Catherine Holloway^{a,b}

^a Interaction Centre (UCLIC), University College London, London, United Kingdom

^b Global Disability Innovation Hub, London, United Kingdom

^c Electrochemical Innovation Lab (EIL), Department of Chemical Engineering, University College London London, United Kingdom

^d Pedestrian Accessibility & Movement Environment Laboratory (PAMELA), Department of Civil, Environmental and Geomatic Engineering, University College London, London, United Kingdom

^e Aspire CREATE (Centre for Rehabilitation Engineering and Assistive Technology), Institute of Orthopedics and Musculoskeletal Science, University College London, Royal National Orthopedic Hospital, United Kingdom

ARTICLE INFO

Keywords:

Batteries
Power wheelchair
Assistive technology
Fuel cell
Drive cycle
Power cycle
Electric wheelchair

ABSTRACT

The implementation of lighter and smaller power sources requires the estimation of power demand under different driving conditions, which are not available for portable assistive technology such as electric or power wheelchairs. Power demand estimated through power and driving cycles is a common methodology in the automotive industry and critical for sizing the power sources. This study determines power and driving cycles in simulated standard outdoor conditions adapting the microtrip methodology. Power consumption and distance travelled were calculated for five different tasks (longitudinal slopes, cross slopes and a flat surface). A “typical” wheelchair journey is presented as a suggested representative drive cycle. A numerical estimation of the power cycle is compared to the experimental results. The difference between numerical and experimental mean and maximum power is 7.58% and 1.07% respectively. Ascending longitudinal slopes were characterized by significantly higher mean power consumption compared to cross slopes and the flat surface. A theoretical fuel cell implementation is presented. The powertrain has a 160 W fuel cell and 470 W battery with a 27 gH₂ metal hydride canister that increases the 30 km original range of the deep-cycle lead acid batteries of the electric wheelchair to 521 km.

1. Introduction

Electric or power wheelchairs have witnessed significant improvements, resulting in the introduction of new designs and functionalities [1] such as pushrim-activated power-assistance [2], stair-climbing [3], standing frames [4] and shared control [5,6]. However, the power source and drive train have not advanced at the same pace, as most commercially available wheelchairs are still limited to the use of deep cycle lead-acid batteries which represent an important restrictive factor in design, due to both high weight and size [7]. Lighter and more efficient Li-ion batteries have been used for both research prototypes [8] and commercially available products like e-bikes [9]; however, concerns related to cost, safety and reliability have prevented wider use [10,11].

Alternative power sources, such as solar and fuel cells, have recently attracted great interests due to important characteristics such as low

weight and hybridization that enables rapid recharging time. This rise of interest in alternative power sources is reflected in the number of publications featuring experimental prototypes of alternatively powered wheelchairs [12–15]. Although these preliminary results appeared quite promising, none of the proposed systems have managed to reach the market and become available to users. This is due to the lack of maturity of the proposed technologies and also due to the lack of basic knowledge about the real-life power requirements of electric wheelchairs.

When selecting, designing and testing power sources for electric vehicles, it is paramount to correctly estimate their power and energy demand under different driving conditions [16,17]. In the automotive industry this is usually achieved through the integration of data from one or more driving cycles. Driving cycles express the variation of speed over time, representing different driving conditions that a vehicle may

* Corresponding author at: UCLIC, Computer Science, University College London, 66-72 Gower Street, WC1E 6BT, London, United Kingdom.

E-mail address: d.morgado-ramirez@ucl.ac.uk (D.Z. Morgado Ramirez).

¹ Joint authorship.

encounter in a specific region or city. They have long been used in the automotive industry to estimate performance, fuel consumption and emissions within a set area or under specific conditions [18]. Unfortunately, data related to electric wheelchair driving cycles are almost non-existent. To our knowledge, Kauzlarich et al. [19] is the only study to investigate electric wheelchair driving cycles and they propose using this methodology for battery testing and selection. Kauzlarich et al. [19] used a wheelchair that was released in 1981, the Power Rolls IV Wheelchair by Invacare, which is now 36 years old, thus no longer representative of electric wheelchairs currently available in the market.

In the automotive industry, first a route is selected based on transport statistics and then different methodologies are used to construct the driving cycle. There is no standardized method to determine the route and different approaches can be taken to establishing the driving cycle.

Route selection is usually done with consideration of the specific purpose of the trip. In some studies, the selection is based on the researchers' judgement, the density of population or road classification. Other methods have considered traffic flow statistics and derived travel speeds in order to select a series of routes which could offer an accurate representation of different driving speeds occurring in the area in which the vehicle might be used [20,21]. Unfortunately, similar data specific to the population of wheelchair users (e.g. pedestrian flows and resulting wheelchair user speeds in different densities of flow) do not exist.

Once suitable data has been collected, different methodologies are adopted to construct the driving cycle. One strategy is to compute an average of the speed-time data recorded and set it as a target statistic. The tests performed are then compared and the cycle representing the closest match to the target values is selected as a representative cycle [22]. This method, while simple, fails to incorporate different behaviors, which could potentially exclude important characteristics such as different acceleration patterns or various levels of driver's aggressiveness in high traffic conditions.

A more flexible alternative to this technique is the microtrip construction method. Data collected from each test are divided into segments based on set criteria, such as idle periods (engine is running, but the vehicle is not moving) or route segmentation based on set distance, time or geographical landmarks. Analysis is performed to find target statistics and representative cycles are selected for each microtrip. Combinations of multiple microtrips into a cycle is often done by random selection, [23]. With the purpose of designing a more inclusive cycle, some studies have pre-defined segments of a route to ensure an inclusive selection of microtrips representing various driving conditions such as highways, congested roads and residential roads. Then a set number of trips from each condition are selected for the final cycle [24]. An example of this method can be seen in Fig. 1. An important step for all the methods presented, particularly when using the microtrip approach, is to establish the length or duration of the driving cycle, which should be both representative and easily repeatable. Depending on requirements, driving cycles can be constructed based on distance travelled or on usage time, and this is usually done using data concerning local average trip length or duration from local transport planning models [23].

The power consumption of vehicles is usually estimated with a model that incorporates the vehicle characteristics with the speed and acceleration calculated from the driving cycles [16,25]. For electric vehicles, this can be accurately measured by the continuous monitoring of voltage and current drawn from the batteries while the driver moves the vehicle along the selected route. This strategy can be used to obtain power cycles in real time [26]. Correctly estimating power consumption is particularly important for electric and hybrid vehicles as the data generated numerically from such analysis can be used to select and size the appropriate power sources without requiring experimental data [25]. An example of a hybrid system is the coupling of a battery with a fuel cell.

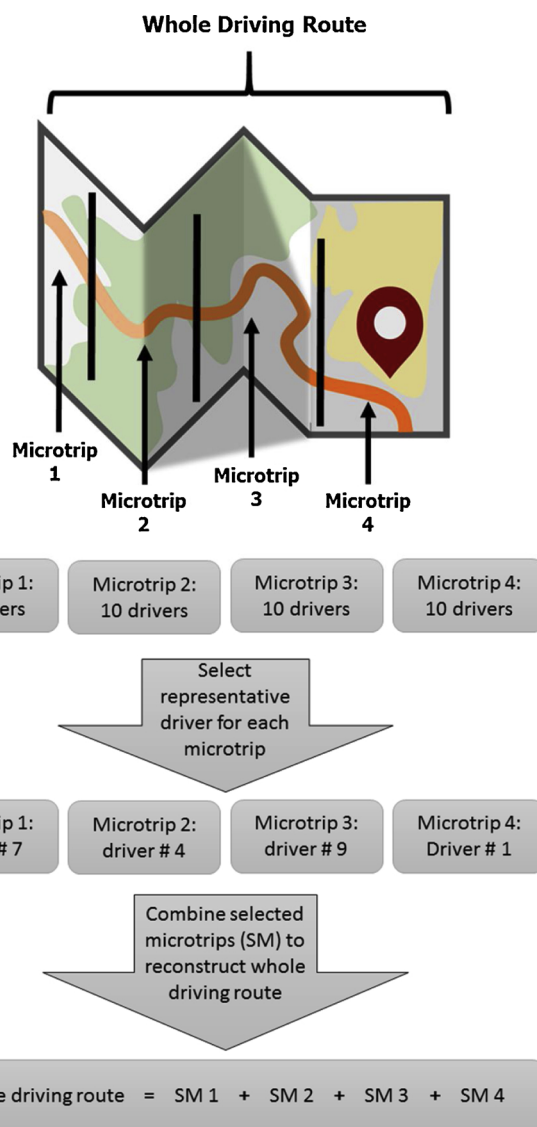


Fig. 1. Example of the Microtrip method where a driving route is repeated by different drivers. The route is divided into sections called microtrips. Representative microtrips are selected and combined to reconstruct a whole driving route. In this example four microtrips are used while in this study five are used.

At the top of the image a map depicts a road and arrows refer to sections of the route on that road which are called microtrips. There are four arrows. Below the example continues to depict a fictitious scenario where 10 drivers did each of the four microtrips. Then a big arrow takes us to the next step by saying “select representative driver for each microtrip”. Thus four blocks follow showing a fictitious selection: microtrip one represented by driver number 7, microtrip 2 represented by driver 4, microtrip 3 represented by driver 9 and microtrip 4 represented by driver 1. A second big arrow takes us to the next step saying “combine selected microtrips (SM) to reconstruct whole driving route”. The final block says: whole driving route equals SM1 plus SM2 plus SM3 plus SM4. End of the image.

Polymer Electrolyte Fuel Cells (PEFCs) are electrochemical devices that convert a feed of hydrogen and oxygen (usually in the form of air) into water, whilst simultaneously generating electrical power [27]. Among the various fuel cell technologies available, PEFCs are the most scalable to desired applications with capacities ranging from mW to MW and are more suited to automotive applications due to their low-temperature operation [27]. Their power density is characterized by the size of the membrane electrode area (MEA), and their energy density is determined by the storage size of hydrogen fuel. Open-cathode

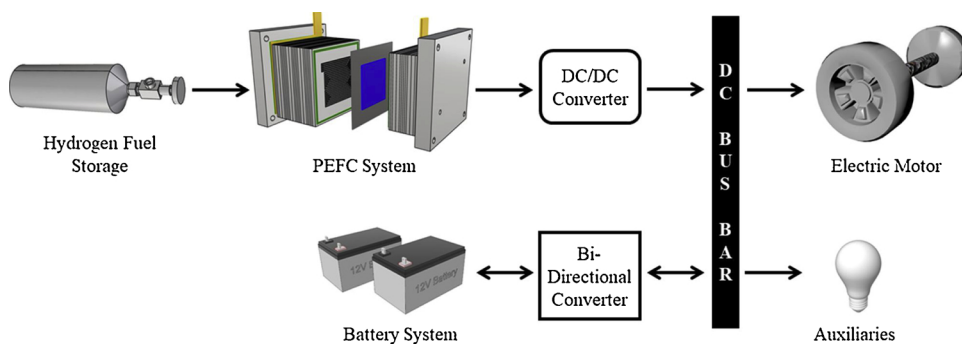


Fig. 2. System architecture of a fuel cell battery hybrid for electric wheelchair applications. Seven elements arranged over two rows. Starting from the left side of the image. At the top row an icon of a hydrogen fuel cell tank with an arrow pointing to the right to the icon of a PEFC system with an arrow to the right to a text box that says “DC/DC converter” with an arrow pointing to the right to a vertical bar, that occupies the two rows mentioned at the beginning, the vertical bar represents a DC bus bar and then another arrow pointing to the right at the level of the first row points to the icon of an electric motor. From left to right now the description of the contents in the second row. The icon of a battery system (which is located right below the icon of the PEFC system mentioned earlier) with a double arrowed line pointing to the left and right, to the right there is a text box that says “Bi-directional converter”. Then another bidirectional arrow points to the right to the DC bus bar and then a single arrow pointing to the right to the icon of a light bulb that represents auxiliaries.

configurations are the most commonly used for small-scale applications where the cathode is open to the atmosphere and blowers are used to both supply the oxygen feed and provide cooling, thus greatly reducing the sub-system requirements for operation. A sub-system is anything that needs to be powered to make the system run.

Disadvantages of this technology include: non-immediate start-up time, limited response time to dynamic load changes and the increased degradation when operated in non-steady-state, away from the design point. Hybridization with other power sources, such as batteries or super-capacitors, can alleviate these stresses on the fuel cell and provide the initial immediate surges in power demand [28].

The architecture of the hybridization will depend on the system’s requirements and can facilitate add-ons such as regenerative braking (where a fraction of the frictional energy lost during braking can be recovered and used to recharge the energy storage devices onboard). Fig. 2 displays a common system architecture used in fuel cell hybrid systems adapted to any device with an electric motor. This configuration facilitates two operational strategies. The first utilizes the PEFC as a range-extender to ‘top-up’ the battery when it is not discharging to the motor; thus, the PEFC size can be small. In the second strategy, the PEFC can be used in conjunction with the battery to power the motor; or can directly power the motor as well as recharge the battery during propulsion if the battery’s state-of-charge is low. A selection is made depending on the electronics complexity or the size of fuel cell selected based on a power cycle derived from a drive cycle. Both configurations can facilitate regenerative braking by reversing the electric motor into a generator, but this design is beyond the scope of our initial investigation.

The aims of this study therefore are to:

- a. Adapt the microtrip methodology to measure the first electric wheelchair power and driving cycles encompassing typical driving conditions, simulated as standard outdoor city conditions.
- b. To use approximating equations to estimate the power demand through the drive cycle and compare it to the experimentally measured power demand, thus evaluating the validity of the proposed adapted microtrip method.
- c. Use the driving cycle to estimate the size of an alternative power source for hybridization using a fuel cell.

2. Methods

2.1. Participant recruitment

The study was approved by the University College London (UCL) Ethics committee. Participants were recruited among UCL students and staff, after informed and signed consent was obtained. Inclusion criteria for the study were people aged between 18–55 years with limited or no experience in electric wheelchair driving.

2.2. Setting

This study was carried out at the UCL Pedestrian Accessibility Movement Environment Laboratory (PAMELA) [29]. The laboratory features a platform with 58 (1.4 m² each) modules that allow the simulation of an urban environment. For this experiment, the platform was divided into five lanes, each one representative of surfaces commonly found in the urban environment (flat surface, cross and

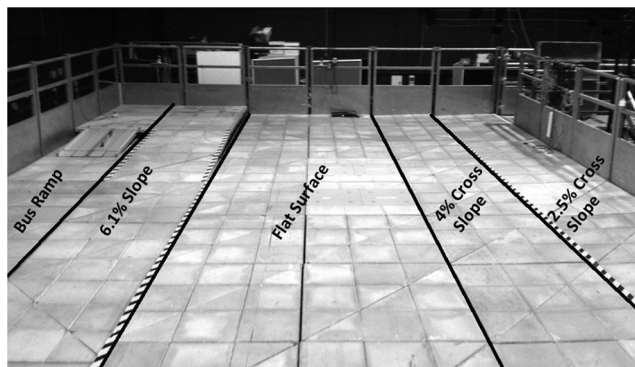


Fig. 3. Five platform paths arrangements where five tasks were performed. Platform settings were representative of the city of London, UK urban environment. From left to right: bus ramp with 12% ascending slope, 6.1% ascending slope, flat surface, 4% cross slope and 2.5% cross slope. From left to right there are five areas marked in the image of the platform of the laboratory where the experiments were performed: bus ramp with 12% ascending slope, 6.1% ascending slope, flat surface, 4% cross slope and 2.5% cross slope. The platform consists in concrete blocks thus the surface resembles a paved footpath. Each block can be raised and/or inclined in order to replicate the desired surface length and inclination.

Table 1

Properties of five selected tasks that each participant repeated three times and the selected microtrips for the UCL-EWDC.

| Task name | Gradient (%) | Distance (m) | Numerical Gradient (°) | Selected microtrips | |
|----------------------|--------------|--------------|------------------------|---------------------|-------------|
| | | | | Trial | Participant |
| Flat surface | 0 | 9.56 | 0 | 1 | 4 |
| Cross slope 2.5% | 2.5 | 9.78 | 0 | 2 | 6 |
| Cross slope 4% | 4 | 9.51 | 0 | 3 | 6 |
| Ascending slope 6.1% | 6.1 | 6.55 | 3.49 | 2 | 3 |
| Ascending slope 12% | 12 | 4.70 | 6.84 | 1 | 2 |

longitudinal slopes). These choices were informed by the Inclusive Mobility guidelines [30], the Accessible Bus Stop Design Guidelines [31] as well as with reference to the work of Beale et al. [32] and Matthews et al. [33]. The platform layout is illustrated in Fig. 3. The details of five selected tasks are in Table 1.

The 12% ascending slope task was selected as the representation of a bus ramp [31]. One meter of clearance and 1 m of landing were given before and after the 12% ascending slope task, resulting in a total distance of 4.7 m. The other surfaces were 35.4 m long in total and consisted of: a flat surface, a 2.5% cross-slope (the UK standard), a 4% cross-slope (often found in UK footways) and a 6.1% slope. Cross-slopes are a common feature of footways and frequently cause problems for wheelchair users [34,35]. All selected tasks were considered representative to simulate average journeys made by wheelchair users within the urban environment. Platform surface was standard concrete pavement typically found in London, United Kingdom footpaths [36].

2.3. Equipment

A Typhoon II electric wheelchair (Invacare Corporation, Elyria, OH) was selected for testing as a representative type of often used electric wheelchairs. The Typhoon II has the following features: 34 cm diameter mid driving wheels, 12 cm diameter front/rear casters, tire pressure 2.8 bar, 48 cm seat width, 51 cm seat depth, 63 cm overall width, 124 cm overall height, 116 cm overall length, 180 kg wheelchair weight and 10 km h^{-1} maximum speed. The two on-board lead-acid batteries were connected electrically in series and rated for 12 V, 60 Ah each, totaling 1.44 kW of nominal output power.

2.4. Experimental protocol

Each task (Table 1) was performed three times by all participants; each repetition is called a ‘trial’ here onwards. Each participant was given 10 minutes prior to the experiment to acclimatize themselves with the wheelchair commands and platform layout. Participants were given an oral command to start the trial when all sensing units were switched on and recording started.

2.5. Data acquisition and processing

A custom designed data logger based on an Arduino Uno microcontroller board (Arduino SRL, Turin, Italy) was used. The mass of the data logger and sensors was 0.3 kg. The data logger was able to record and store on the micro SD card the voltage and current drawn from the batteries. A linear split core Hall Effect sensor LDS050-SP-5 V was used to measure current (Loulensy Inc., China). This sensor has a measurement range of 0–50 A DC with 1% accuracy. Voltage was monitored through a current shunt on the DX-Bus plug and socket. Power consumption was calculated by the data logger according to Ohm's law. The sampling frequency of the system was set at 100 Hz. Driving wheels rotational speed was measured using two XSens MTw inertial measurement units (IMUs), one placed on each wheel center (XSens Technologies, NL). IMUs sampling frequency was set at 100 Hz. The

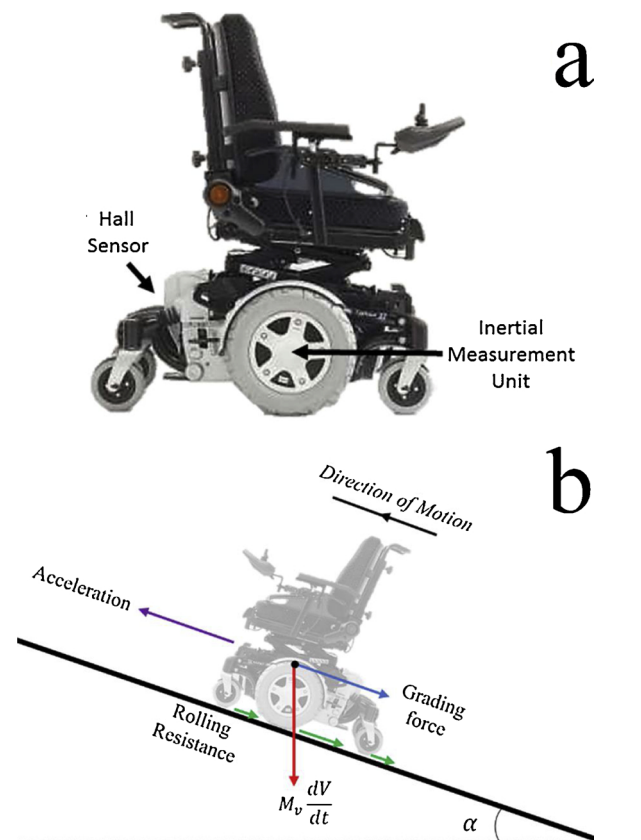


Fig. 4. (a) Electric wheelchair with indicated locations of inertia measurement units and hall sensor. (b) Predominant resistive forces acting on an electric wheelchair climbing an inclined slope.

There are two elements in this figure. At the top there is the photograph of the electric wheelchair used in this study, with indicated locations of inertia measurement units at the center of the bigger wheels and hall sensor at the back of the wheelchair where the battery pack is located. At the bottom of the image there is a line depicting the inclination of a surface and a smaller photograph of the same wheelchair over the depicted inclined line. The image has arrows indicating the forces acting in the system. These forces are: vertical in the negative direction (down) vehicle mass, grading force with an arrow pointing in the opposite direction to the front of the wheelchair, acceleration depicted with an arrow in the direction of the front of the wheelchair or ahead of it and direction of motion which is to the front of the wheelchair or to what is ahead of it. Finally, the angle of the inclined surface to the horizontal is depicted by the angle alpha.

location of sensors on the wheelchair can be seen in Fig. 4 (a). Timestamp synchronization was performed to allow comparison of the collected data. The recordings from the data logger and the IMUs were transferred to a personal computer and custom-built MATLAB scripts were implemented for analysis (R2015A The MathWorks Inc, MA, USA). Power data was first filtered with a moving average filter with a window size of 100 and then low pass filtered with a zero phase 5th

order Butterworth algorithm with a 1 Hz cut off frequency.

The distance travelled was calculated from the wheels’ rotational speed. The wheelchair speed was calculated from the distance travelled and low pass filtered with a zero phase 5th order Butterworth algorithm with a 1 Hz cut off frequency.

2.6. Data analysis

Mean (*M*) and maximum (*Max*) power for each trial, each participant and each task were computed. Then mean power (M_p) for each task was calculated by averaging the results across all trials and participants for each task. The latter represents the target values against which microtrips from each participant were measured in order to identify the most representative one. Median Absolute Deviation (MAD) between *M* for each participant and *Max* was calculated. The smallest MAD value for each task was chosen as the representative microtrip. Power readings of selected microtrips were then paired with respective speed data. This step was considered fundamental in order to combine single microtrips into a complete drive cycle. The effect of cross and longitudinal slopes compared to the flat surface task on *M* and *Max* power consumption was verified using Kruskal-Wallis independent sample tests with Bonferroni correction for multiple tests at a significance level of 0.05 and 95% confidence interval.

The methodology followed to construct a drive cycle was based on the microtrips approach where each task is performed and examined separately as a specific driving condition. Microtrips can be combined to create many drive cycle possibilities depending on the cycle distance chosen. A series of microtrips were chosen and then combined based on a selected distance covered by the wheelchair. The total distance covered was arbitrarily set to approximately 66 m (216.5 ft). Integers from 1 to 5 were assigned to each task and a series of randomly generated numbers were used for the combination. In this study, the power cycle was constructed from the calculated power based on the Hall sensor measurements. The drive cycle was calculated from the speed calculated based on the distance travelled by the wheelchair measured through the IMUs.

3. Results

3.1. Participants

Eight participants volunteered for this study. Participants’ age ranged from 22 to 47 years, with a mean ± SD of 32.6 ± 7.7 years. Participants’ weight ranged from 63 to 94 kg, with a mean ± SD of 74.6 ± 10.8 kg. The characteristics of each participant are presented in Table 2.

3.2. Power

M and *Max* power distribution and medians are presented in Fig. 5. M_p for each task are 54.0, 56.5, 129.2, 132.8 and 58.2 W for flat, 4%, 6.1%, 12% and 2.5% respectively.

Table 2

Participant characteristics.

Table has four columns (participant number, weight in kilograms, height in centimeters and age in years) and eight rows for each participant.

| Participant | Weight (Kg) | Height (cm) | Age (years) |
|-------------|-------------|-------------|-------------|
| 1 | 80 | 195 | 33 |
| 2 | 75 | 170 | 29 |
| 3 | 84 | 167 | 30 |
| 4 | 63 | 176 | 29 |
| 5 | 70 | 168 | 31 |
| 6 | 63 | 174 | 47 |
| 7 | 94 | 188 | 40 |
| 8 | 68 | 176 | 22 |

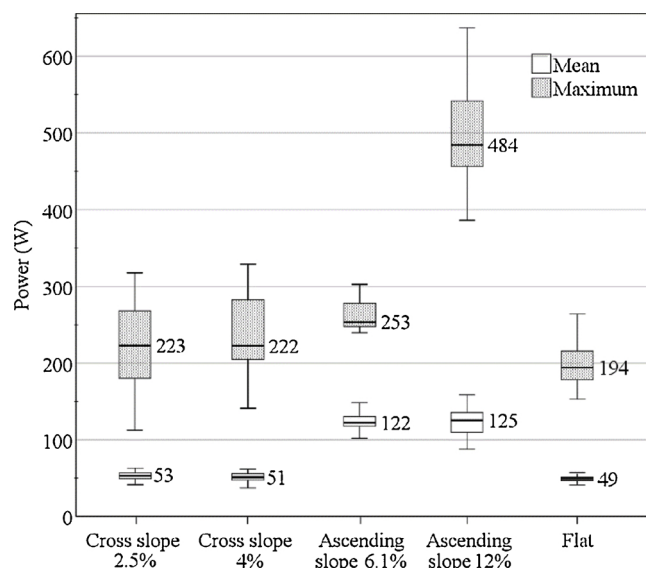


Fig. 5. Mean and maximum power distribution across the five tasks performed. Median values shown.

Where Fig. stands for Figure. Figure is a plot with each of the five tasks on the horizontal axis and power in Watts in the vertical axis presented every 100 Watts from 0 Watts up to 650 Watts. Inside the plots there are two boxes, each with a horizontal line inside depicting the median. Each box for each activity represent the distribution of mean and the maximum values with confidence intervals. Confidence intervals are represented by a vertical line at the top and at the bottom of each box. All boxes are of different sizes. Median values also appear on the right side of each box. On the horizontal axis, the order of the tasks presented is crossslope 2.5%, cross slope 4%, ascending slope 6.1%, ascending slope 12% and flat.

M power of the flat surface was significantly lower when compared to both longitudinal ascending slopes but not cross slopes. *M* power of both cross slopes were significantly lower when compared to both longitudinal ascending slopes. *Max* power of the flat surface was significantly lower when compared to both longitudinal ascending slopes. *Max* of both cross slopes were significantly lower when compared to the 12% longitudinal ascending slope. *Max* power of the 12% longitudinal ascending slope was significantly higher when compared to the 6.1% slope. All significant values were lower than 0.01.

For the selected microtrips, the participant’s trials are presented in Table 1. Power and speed of the selected microtrips are shown in Fig. 6.

Three of the examined tasks (Fig. 6, a, b and e) show a similar trend with maximum power consumption at the beginning of the trial, which is needed to overcome the inertia of the wheelchair, followed by a significantly lower and steadier power while the wheelchair is travelling. Slope ascending at 12% showed two separate peaks of power due to the acceleration moving on to the ramp itself and then clearing the ramp (Fig. 6, d). Distances travelled by the wheelchair during each trial are shown in the appendix.

3.3. Power and drive cycles

By connecting together the experimentally determined power of the selected microtrips (Fig. 6), the UCL-EWPC (UCL Electric Wheelchair Power Cycle) is produced (Fig. 7). By connecting together the speed profile of the selected microtrips (Fig. 6), the UCL-EWDC (UCL Electric Wheelchair Drive Cycle) is produced (Fig. 7). Between each microtrip, the wheelchair was assumed to completely stop, as shown by the speed reaching zero (Fig. 6). Alternative drive cycles can be constructed, if the example given is not tailored to the reader’s experimental requirements, using the microtrips data (speed, power and time) provided in the supplementary data. The UCL-EWPC can be used to approximate the time-varying load on batteries. The UCL-EWDC can be used to predict a

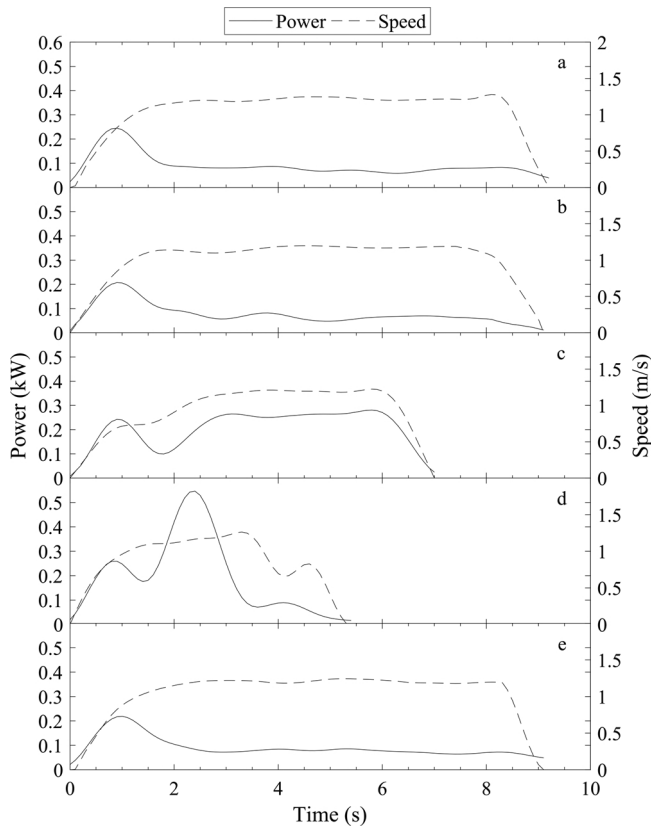


Fig. 6. Power readings and calculated speed for selected microtrips: (a) cross slope 2.5%, (b) cross slope 4%, (c) ascending slope 6.1%, (d) ascending slope 12%, (e) flat surface.

At the horizontal axis there is time in seconds, at the left vertical axis there is power in kilowatts and at the right axis there is speed in meters per second. There are five horizontal sections for the figure, each depicting two curves for each microtrip: cross slope 2.5%, cross slope 4%, ascending slope 6.1%, ascending slope 12% and flat surface. For each microtrip one curve represents power and the other speed.

power cycle using equations and then compared with the power cycle determined experimentally in this study.

4. Numerical validation

The numerical estimation implemented here is based on well-established vehicle dynamics equations [37]. These sets of equations are used to transform the drive cycle presented in this paper into a power

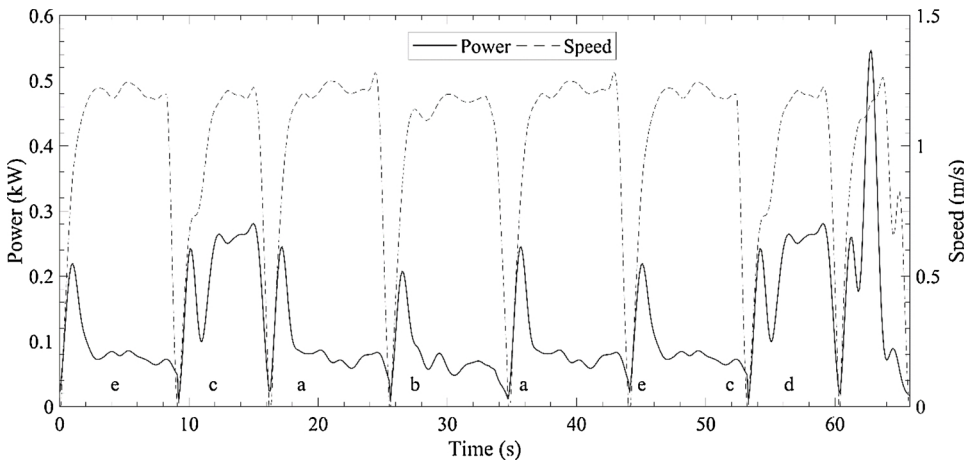


Fig. 7. Experimental electric wheelchair power cycle and drive cycle (speed) for selected microtrips: (a) cross slope 2.5%, (b) cross slope 4%, (c) ascending slope 6.1%, (d) ascending slope 12%, (e) flat surface.

At the horizontal axis there is time in seconds, in the left vertical axis there is power in kilowatts and in the right vertical axis there is speed in meters per second. There are two lines in one plot, one continuous which is the power and the other the speed.

cycle. It is possible to use the microtrips presented here to build application-specific power cycles to estimate the power demands of other electric wheelchairs.

When any vehicle is in motion, there are resistances opposing its movement and concerning electric wheelchairs, tire resistance to the road and acceleration resistance are predominant. The total resistance to motion (F) considered for electric wheelchairs is presented in Eq. (1), where the first contribution is due to the road resistance and the second the acceleration.

$$F = \begin{cases} M_v g (f_r \cos \alpha + \sin \alpha), & \frac{dV}{dt} < 0 \\ M_v g (f_r \cos \alpha + \sin \alpha) + M_v \frac{dV}{dt}, & \frac{dV}{dt} \geq 0 \end{cases} \quad (1)$$

This equation incorporates the vehicle mass (M_v), gravity (g), the rolling resistant coefficient (f_r), which is a function of the tire and road material, the speed of the wheelchair (V) and the slope of the road surface (α). See Fig. 4 (b). Aerodynamic resistances are neglected as the results are negligible due to the low speed of the wheelchair. Automotive applications consider the frictional braking losses defined by a deceleration in the second term of the equation, which can be back-calculated to find the energy obtainable for regenerative braking. With electric wheelchairs, there is a reduction in power transmitted to the motor over any braking forces, because they are push-activated, thus the deceleration term is not considered, and the power term associated to this deceleration is set to 0 W, as explained in Eq. (1).

The slope of the road surface is given in this analysis as a grade value (ϑ) and requires conversion to degrees using Eq. (2). Note that the cross slopes, 2.5% and 4%, are not considered as an inclined slope in the calculations and are thus set to 0° due to the added complexity in numerical estimation if considered.

$$\alpha = \tan^{-1}\vartheta \quad (2)$$

After calculating the forces acting on the wheelchair during motion, the power drawn from the battery (P_E) is estimated.

$$P_E = FV \eta_t^{-1} \quad (3)$$

The efficiency of the motor (η_t) is considered in Eq. (3), which considers energy loss due to predominantly heat and frictional losses [38]. Whilst Eq. (3) approximates the power required for motion, an extra 5 W is added in Eq. (4) to represent the parasitic loads for the electric wheelchair accessories, determined experimentally when the wheelchair was stationary.

$$P = P_E + 5 \quad (4)$$

Equations (1) to (4) can be applied to all the microtrips, excluding the 12% ascending slope. This microtrip, resembling a bus ramp, has a varying gradient which is emulated in Eq. (5) where a transition from a flat surface, on to the inclined slope and then back to flat are taken into

account.

$$\alpha = \begin{cases} 0\%, & 0 \leq t \leq 1.3s \\ 0 \text{ to } 12\%, & 1.4 \leq t \leq 2.3s \\ 12\%, & 2.4 \leq t \leq 2.5s \\ 12 \text{ to } 0\%, & 2.6 \leq t \leq 3.5s \\ 0\%, & 3.6 \leq t \leq 5.4s \end{cases} \quad (5)$$

The original data was separated based on distance travelled before and after the ramp, but for ease of calculation, this has been replaced here with time and is grouped with the microtrip data in the supplementary data.

The numerical parameters for the Typhoon II electric wheelchair are: a mass of 249.75 kg, rolling resistant coefficient of 0.13 and a motor efficiency of 0.75. The mass was calculated as the average of the passenger weights of each microtrip selected for the drive cycle in addition to the wheelchair weight. The rolling resistance coefficient was valued for car tires on concrete or asphalt [37], the most comparable to the conditions experienced by electric wheelchairs on UK roads. The efficiency of the Typhoon II motors was not found in the specifications; however, a value was chosen based on typical efficiencies of electric motors in literature [38]. The obtained numerical estimation of the power cycle based on the experimentally calculated drive cycle is presented in

Fig. 8. It is also presented with the power cycle obtained experimentally, for comparison.

During the simulation, the validity of the numerical assumptions was assessed. The cross slopes were comparable in power consumption to the flat surface trip, attested by the curve shape similarity and magnitude between a, b and e in Fig. 6. Cross slopes were calculated as flat surfaces. The omission of the deceleration term proved vital in achieving similar results between the numerical simulation and the experimental power results. Other assumptions included: only forward wheelchair propulsion, smooth roads/paving, center of mass positioned in the middle of the wheelchair and the omission of extreme weather considerations.

The numerical and experimental power curves for each microtrip are compared in Table 3, by analyzing the differences in average and maximum power using Eq. (6).

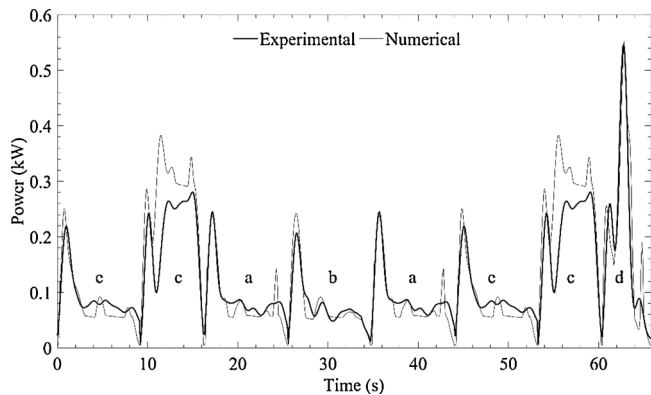


Fig. 8. Numerical estimation of power cycle based on the experimentally calculated electric wheelchair drive cycle. Also, the corresponding experimental power cycle. Based on the selected microtrips: (a) cross slope 2.5%, (b) cross slope 4%, (c) ascending slope 6.1%, (d) ascending slope 12%, (e) flat surface. There are two lines, one continuous which is the experimental drive cycle and a dotted line which represents the numerical estimation of the power cycle. numerical estimation of power cycle based on the experimentally calculated electric wheelchair drive cycle. Also, the corresponding experimental power cycle. Based on the selected microtrips: (a) cross slope 2.5%, (b) cross slope 4%, (c) ascending slope 6.1%, (d) ascending slope 12%, (e) flat surface. Microtrips in the plot are presented in the following order e, c, a, b, a, e, c and d. At the horizontal axis there is time in seconds and in the vertical axis there is power in Watts.

$$\% \text{ difference} = \frac{\text{numerical} - \text{experimental}}{\text{numerical}} \times 100 \quad (6)$$

The total combined power cycle in Fig. 8, gave a small overall difference between numerical and experimental, with the average 7.58% different and the maximum values 1.07%. It was assumed that a difference in power values of $\pm 20\%$ was reasonable due to the simplicity of the numerical equations. Mann Whitney U tests with a 95% confidence interval and 0.05 significance were performed, for each microtrip, to compare the experimental and the numerical power. Flat surface, 6.1% longitudinal ascending slope and 2.5% cross slope were significantly different. Differences in power estimation after the initial acceleration peak may be due to the sensitivity of the numerical equations with changing speed.

5. Theoretical implementation example

The minimum power output for a PEFC in a drivetrain is calculated as the mean power requirement of the electric wheelchair over the drive cycle lifetime. For the experimental drive cycle in Fig. 7, this is 131.3 W. However, it is desirable to increase the power design of the fuel cell, to allow it to assist the wheelchair comfortably during high constant speeds and common road inclines [37]. A correction factor of 20% was applied to the minimum power output (resulting in ≈ 160 W) to accommodate for the simplification of the equations. Typically, in the automotive industry, a correction factor is applied to the power values of at least 20%, which compensates for errors and ensures the engine sizes are not under-specified in design. Thus the numerical results are deemed reasonable and the error is acceptable for determining the size of the powertrain components.

After determining the minimum power output for a PEFC in a drivetrain, the battery system coupled with it is sized to assist in delivering the 552.4 W maximum power load (numerical power, Table 3). Including a 20% correction factor to 552.4 W it becomes a 470 W battery. If two lead-acid batteries are chosen and connected in series, the capacity of each battery will drop from the original 60 Ah in the Typhoon II to below 20 Ah in this new PEFC drivetrain. This represents a 67% decrease from the original nominal power rating of the Typhoon I (1.44 kW) to the proposed hybrid wheelchair battery pack.

The powertrain design can be flexible, and whilst a minimum power requirement from the fuel cell has been specified, a trade-off between fuel cell size, battery size and architectural complexity can be optimized for weight, volume and cost. In the case of the electric wheelchair, all three variables are key for the successful commercialization of the hybridized system.

By increasing the fuel cell power, the weight and cost of the batteries can be reduced but at the cost of a reduced back-up range if hydrogen fuel is depleted. Deep-cycle lead-acid batteries are commonly used in electric wheelchairs because of their low cost whilst maintaining a modest high efficiency (70%), cycle life (1000) and power density (100 Wkg^{-1}) [39]. In the original Typhoon II power pack arrangement, the 12 V 60 Ah batteries weigh approximately 40 kg, which represents 20% of the total weight of the wheelchair. Li-ion batteries have superior performance to the lead-acid, with a higher power density (1800 Wkg^{-1}), energy density (100 Whkg^{-1}) and efficiency (80%) [39]. Thus, the Typhoon II original lead-acid battery pack without fuel cell assistance, could be replaced with a Li-ion system that weighs 60% less for the same range (based on calculation with energy density shown in Eq. (7) and have a greater cycle lifetime for the same electrical requirements.

$$M_{Li-ion} = 1440(Wh)/100(Wh \text{ kg}^{-1}) = 14.4 \text{ kg} \quad (7)$$

Li-ion has drawbacks such as thermal safety issues, capacity deterioration after one year of operation and its far greater cost [40]. A trade-off can be established by adding a fuel cell to the powertrain, thus reducing the size of the Li-ion system and making the electric

Table 3

Comparison of experimental and numerical results obtained for the power cycle of each microtrip and the total conversion of the UCL-EWDC.

There are seven columns: task name, mean and maximum experimental power in watts, mean and maximum numerical power in watts and mean and maximum percentage difference between experimental and numerical power. There are six rows, five for each task and an additional row for the total cycle.

| Task name | Experimental power (W) | | Numerical Power (W) | | Percentage Difference (%) | |
|----------------------|------------------------|---------|---------------------|---------|---------------------------|---------|
| | Mean | Maximum | Mean | Maximum | Mean | Maximum |
| Flat surface | 90.70 | 219.09 | 81.37 | 250.53 | –11.46 | 12.55 |
| Cross slope 2.5% | 91.17 | 245.06 | 83.88 | 237.90 | –8.69 | –3.01 |
| Cross slope 4% | 75.99 | 207.16 | 78.07 | 242.36 | 2.67 | 12.52 |
| Ascending slope 6.1% | 203.08 | 280.64 | 266.25 | 382.61 | 23.73 | 26.65 |
| Ascending slope 12% | 191.10 | 546.43 | 199.72 | 552.36 | 4.32 | 1.07 |
| Total Cycle | 121.37 | 546.43 | 131.33 | 552.36 | 7.58 | 1.07 |

wheelchair more affordable and lightweight with extended lifetime and reliability.

Now the range expected from a single commercial hydrogen metal hydride canister can be deduced. For an electric wheelchair, a 24 V operational output is desirable from the PEFC; matching the charging voltage of the on-board batteries and reducing efficiency losses in DC/DC converters. By dividing the minimum PEFC power output calculated previously (160 W) by 24 V, a 6.7 A output is obtained. Faraday's law in Eq. (8) can be used to calculate the amount of H₂ consumed (\dot{M}_{H_2}) for the wheelchair to complete one cycle of the UCL-EWDC [37].

$$\dot{M}_{H_2} = \frac{i}{nF} M_{r,H_2} = \frac{6.7}{2 \times 96485} 2.016 = 3.47 \times 10^{-5} \text{gs}^{-1} \quad (8)$$

Here, n is the number of electrons transferred, F is Faraday's constant and M_{r,H_2} is the molecular weight of hydrogen gas. This result is multiplied by a stoichiometric factor of 1.5 to give $5.2 \times 10^{-5} \text{gs}^{-1}$, used to supply more hydrogen than the reaction requirement, to ensure hydrogen depletion and large pressure drops do not occur inside the PEFC. The total run time of the UCL-EWDC is 65.8 s and multiplying this by the mass flowrate requires $3.42 \times 10^{-3} \text{gH}_2$ per cycle. The MH300-A metal hydride canister (Pragma Industries, France) has been selected as an example here and has a H₂ capacity of 27 g, 300 N L with 3 kg total weight [41]. This capacity enables 7895 UCL-EWDC cycles and a total theoretical range without the back-up battery to 521 km, a large increase from the Typhoon II electric wheelchair range of 30 km.

6. Discussion

The microtrip method has been adapted to construct drive and power cycles for electric wheelchairs. Guidelines for implementation and examples from experimental evaluation are provided. Microtrip data is provided as supplementary data so that bespoke drive cycles can be created for specific use cases (i.e. multiple side slopes and bus ramps, specific styles of driving). In addition, those power cycles are necessary for the evaluation of alternative power sources that could benefit a wider spectrum of powered assistive devices. For instance, manual wheelchair users have identified the need to reduce the weight and increase the efficiency of power assistive devices [2].

Electric wheelchairs often represent the primary means of independent mobility for those unable to manually propel a wheelchair. For this reason, they need to be versatile enough to cope with different types of environmental conditions [42]. Due to the need of flexibility required when modelling the usage of electric wheelchairs, a microtrip approach was employed in which different driving conditions are examined separately and combined at a later stage to form a more complex driving cycle [23]. Five representative driving conditions were selected, including flat surface, cross slopes and ascending slopes.

Power readings were first examined separately for each task and target statistics were calculated in order to identify the most representative trials for each condition. Different demands posed by the selected tasks were reflected in the different values for both maximum and mean power readings. As expected, both ascending slopes were

characterized by significantly higher mean power consumption, while smaller differences were found between the two cross slopes and the flat surface. All trials were performed with the wheelchair starting from a static position (stop). The main peak of power appears to be due to the power required to overcome inertia for movement. Once representative microtrips were selected for all conditions, the chosen power readings in relation to the wheelchair speed were analyzed. Although speed appears nearly identical across all examined tasks, variations in the power cycle can be observed across the various conditions. This is an important distinction from automotive drive trains where fuel consumption is usually calculated combining the vehicle's characteristics with the speed profile measured during the driving cycle. Our approach is based on the direct calculation of power cycles for electric wheelchairs rather than an indirect estimation of power consumption based on the drive cycles. The numerical simulation of the power cycle based on the drive cycle has produced a power cycle that is in agreement with the one obtained experimentally.

Comparison of the results with previous work is difficult because the powertrain properties chosen are different to anything published in the past. However, it is important to note that previous work has suggested various hybrid power sources but without justifying the requirements and the design through an electric wheelchair drive cycle [12–15]. Takahashi, Matsuo and Kawakami [13] built a hybrid electrical robotic wheelchair with a 100 W fuel cell, two solar panels of 43 W, and a nickel-hydrogen 24 V battery. Gaps in their work are: unknown weight of the wheelchair, it is unknown if they tested the operation of the wheelchair remotely or if there was a human operator seating in the wheelchair and they measured current consumption at three different speeds but did not calculate a power cycle from that. They reported a power consumption of 50 W during what they call "running" (probably fast straight line displacement of the wheelchair, but no speed was specified), 90 W during turning and 100 W when the wheelchair was gaining inertia for movement. It is difficult to compare these values with the results of our study because of the weight of the unknown variables mentioned and because they used a significantly different wheelchair to the Typhoon II. Takahashi, Matsuo and Kawakami [13] tested a driving condition we did not measure (turning), but their test was after building the hybrid system without a typical electric wheelchair drive cycle as a reference. Thus it is only left to assume that their powertrain may not be fit for purpose.

Similarly, Wang and Chiang [15] designed a fuel cell powered wheelchair. They selected a 500 W PEMFC based on the wheelchair manufacturer's reported rating (100–180 W) and maximum power (300 W) instead of a driving cycle.

Bouquain, Blunier and Miraoui [12] presented a prototype electric wheelchair base with a 300 W PEFC and a lead-acid battery. Their reason for the selected fuel cell is unknown. They mentioned the importance of taking into account the dynamics of a vehicle in order to calculate the driving cycle of an electric wheelchair. However, they did not present such driving cycle that enabled them to reach a power requirement of 400 W.

In summary, previous work seems to have overestimated the fuel cell power requirements, except for Takahashi, Matsuo and Kawakami [13]. We are proposing a 160 W fuel cell with a 470 W battery and a 27 gH₂ metal hydride canister to be sufficient for an electric wheelchair that appears to be considerably bigger and heavier to the ones tested by previous work [12–15].

Yang and Guan [14] proposed a hybrid fuel cell powertrain for a power assist device that converts a manual wheelchair into an electric one, operated through a joystick. In contrast with previous work, they tested various driving patterns but did not explain them and only captured the time to reach peak, “cruise” and average power. They found that 678 W was needed for a wheelchair to accelerate up a slope and 305 W to cruise. Their method looked at individual activities and power values at specific times, which may not be representative of driving styles. They chose a 400 W PEMFC, a 240 L hydrogen canister and lithium ion phosphate battery packs. Their research is unique in that it demonstrates the possibility to develop new lighter and more efficient power sources for mobile assistive technology beyond electric wheelchairs, as is the case in their work on a power assisted manual wheelchair. We believe that improving on the work of Yang and Guan [14], by implementing the methodology proposed in this study, will enable the improvement of current power assist devices that is truly fit for purpose. For instance, power assist devices have been identified to be too heavy for manual wheelchair users [2] and dangerous for the stability of the manual wheelchair [43].

As explained above, all past studies have utilized wheelchairs from different manufacturers compared to the Typhoon II utilized in this study. However, we are proposing a methodology that enables the calculation of a drive cycle for any type of electric wheelchair and potentially any other type of mobility assistive devices that use batteries. Thus, this study is presenting transferable methods in contrast with previous studies that are wheelchair specific. We strongly recommend that future research considers the users’ needs, their driving styles and different conditions in which they drive before designing and testing new hybrid power systems.

For the proposed PEFC-battery powertrain, it is important that weight, volume and cost is reduced to avoid increasing the cost of electric wheelchairs. The sizing method proposed here can be used as an estimation of the powertrain components based on the system architecture stated; however, a degree of flexibility is accepted. Additionally, the PEFC sub-system would be the same size independent of PEFC power output for the wheelchair power range, which is a parameter to consider in terms of volume optimization. For reasons of power utilization, the proposed architecture is the best solution for this system as it can greatly reduce the battery size. Possible modes of power operation for this system include:

- a) Start-up: battery powers sub-system and control system to get gases flowing to the PEFC.
- b) Dynamic loads: battery can power the initial surge of demand with the PEFC assisting or taking over once it has safely ramped up to the required power.
- c) Low power demand: PEFC powers system and charges battery simultaneously. If the battery is fully charged, then PEFC is switched off and battery discharges to load until battery discharges below set state-of-charge (SOC) and PEFC is restarted.
- d) High power demand: Both PEFC and battery simultaneously feed the system.
- e) Stand-by: PEFC charges the battery if required.

The implementation example has demonstrated a way of integrating a fuel cell system into an existing commercially available electric wheelchair. Regenerative braking was not considered for this system design because it was not within the scope of this study. A future study focusing on the braking behavior patterns of electric wheelchair users and the amount of frictional energy that could be recovered to recharge

the battery is recommended to validate the implementation of regenerative braking.

The powertrain example proposed, has a 160 W fuel cell and 470 W battery with a 27 gH₂ metal hydride canister. This new design decreased the battery pack’s mass by 88% if kept as lead-acid batteries and increased the wheelchair range from 30 km to 521 km. However, this new range does not include the additional battery back-up range if the wheelchair user runs out of H₂, assuming the batteries are fully charged. The method outlined here does not restrict the design of the PEFC-battery hybrid. If the PEFC size was doubled, the energy capacity of the batteries could be greatly reduced; however, the power density would need to be maintained to ensure transient and start-up power demands are met. Further information on management strategies for hybrid systems can be found elsewhere [44–46] where wheelchairs and scooters are often referred as light traction vehicles [47]. Some of these sources must be used with caution since they are catered to heavy duty vehicles.

When driving cycles are constructed for the automotive industry, the combination of microtrips is regulated by attributing different probabilistic weights to various driving conditions based on data extracted by traffic flow surveys [15]. Unfortunately, such databases are not available for electric wheelchairs. For this reason, different probabilistic weights were not attributed to the road conditions examined. Yet, we believe that the combination of the microtrips can be used to build a model of the experience of full trips. Thus, numbers from 1 to 5 were arbitrarily assigned to all tasks, according to the order in which they are presented in the methods section, and random number generation was used to set the order of the microtrips combination.

In future studies, additional representative driving cycles should be built based on a variety of conditions, including accessibility barriers that are commonly encountered by electric wheelchair users (i.e. descending longitudinal slopes, turning, uneven terrain, crowded spaces). It is very likely that turning will represent a large power demand. Baseline selection could be centered on specific road features that have been identified by participants with various disabilities in previous studies [32,33]. An example of these features are curbs and drop curbs.

Other limitations of this study are related to the fact that the participants recruited did not have any experience in driving electric wheelchairs. Although this did not directly affect the results, as no maneuverability task was included in the analysis, driver’s skill will likely play an important role when more complex driving scenarios are examined. Additionally, the effect that pedestrian traffic flow and static obstacles was not considered and these might have an effect on driving behavior and related power consumption. Future studies will focus on gathering real outdoor data for different populations of wheelchair users to characterize more general and realistic power requirements.

Due to the short distance of the 12% ramp, this test was always considered as if it was preceded and followed by a complete stop of the wheelchair. This is not a limitation because short and steep ramps are often used to allow access to otherwise inaccessible buildings or public transport vehicles. These ramps are often narrow and they are also provided with small landing areas at the top, forcing wheelchair users to perform a complete stop before and after the ramp itself.

7. Conclusion

This study is the first to formulate a flexible approach aimed at modelling driving cycles and measuring power cycles of electric wheelchairs. The microtrips methodology will allow a realistic estimation of power consumption based not only on the characteristics of the wheelchair but also taking into account specific requirements that different driving conditions and styles might impose. We hope future wheelchair designs will be able to make use of our findings to identify the specific needs of powered wheelchair users and help direct research towards alternative power sources better suited to the real needs of the users’ population.

Acknowledgements

Engineering and Physical Sciences Research Council grant number EP/N022971/1.

Appendix A. Supplementary data

Appendix A contains a figure of the distances calculated for each microtrip and a Ragone plot. The data associated with this research paper is available to download by anyone without any requirement through the UK Data Service ReShare [48]. The data contains the microtrip data used to create the power cycle, which the readers can use to build their own power cycle to fit more complex driving needs. Supplementary material (appendix A) to this article can be found in the online version at doi: <https://doi.org/10.1016/j.est.2019.01.027>.

References

- [1] R.A. Cooper, R. Cooper, M.L. Boninger, Trends and issues in wheelchair technologies, *Assist. Technol.* 20 (2) (2008) 61–72.
- [2] D.Z. Morgado Ramirez, C. Holloway, But, I don't want/need a power wheelchair, Proceedings of the 19th International ACM SIGACCESS Conference on Computers and Accessibility (2017) 120–129.
- [3] S.A. Sundaram, et al., Step-climbing power wheelchairs: a literature review, *Top. Spinal Cord Inj. Rehabil.* 23 (2) (2017) 98–109.
- [4] J. Leaman, H.M. La, A comprehensive review of smart wheelchairs: past, present, and future, *IEEE Trans. Hum. Syst.* 47 (4) (2017) 486–499.
- [5] C. Ezech, et al., Comparing shared control approaches for alternative interfaces: a wheelchair simulator experiment, 2017 IEEE International Conference on Systems, Man, and Cybernetics (SMC), (2017).
- [6] D.A. Abbink, et al., A topology of shared control systems—finding common ground in diversity, *IEEE Trans. Hum. Syst.* 48 (5) (2018) 509–525.
- [7] M.R. Palacín, Ade Guibert, Why do batteries fail? *Science* 351 (2016), <https://doi.org/10.1126/science.1253292>.
- [8] R. Hou, X. Shi, M. Krishnamurthy, Design and implementation of a novel power assisted drivetrain for a wheelchair, 2012 IEEE Transportation Electrification Conference and Expo (ITEC), (2012).
- [9] M. Weiss, et al., On the electrification of road transportation – a review of the environmental, economic, and social performance of electric two-wheelers, *Transp. Res. D Transp. Environ.* 41 (2015) 348–366.
- [10] B. Scrosati, J. Garche, Lithium batteries: status, prospects and future, *J. Power Sources* 195 (9) (2010) 2419–2430.
- [11] L. Lu, et al., A review on the key issues for lithium-ion battery management in electric vehicles, *J. Power Sources* 226 (2013) 272–288.
- [12] D. Bouquain, B. Blunier, A. Miraoui, A hybrid fuel cell/battery wheelchair-modeling, simulation and experimentation, 2008 IEEE Vehicle Power and Propulsion Conference, (2008).
- [13] Y. Takahashi, S. Matsuo, K. Kawakami, Hybrid robotic wheelchair with photo-voltaic solar cell and fuel cell, ICCAS, (2008) International Conference on Control, Automation and Systems, 2008.
- [14] Y.P. Yang, R.M. Guan, Hybrid fuel cell powertrain for a powered wheelchair driven by rim motors, 2011 International Conference on Power Engineering, Energy and Electrical Drives, (2011).
- [15] F.-C. Wang, Y.-S. Chiang, Design and control of a PEMFC powered electric wheelchair, *Int. J. Hydrogen Energy* 37 (15) (2012) 11299–11307.
- [16] P. Lazari, J. Wang, L. Chen, A computationally efficient design technique for electric-vehicle traction machines, *IEEE Trans. Ind. Appl.* 50 (5) (2014) 3203–3213.
- [17] B. Lin, Conceptual design and modeling of a fuel cell scooter for urban Asia, *J. Power Sources* 86 (1–2) (2000) 202–213.
- [18] T.J. Lyons, et al., The development of a driving cycle for fuel consumption and emissions evaluation, *Transp. Res. Part A Gen.* 20 (6) (1986) 447–462.
- [19] J.J. Kauzlarich, et al., Wheelchair batteries: driving cycles and testing, *J. Rehabil. R. & D* 20 (1) (1983) 31–43.
- [20] S. Tamsanya, S. Chungpaibulpattana, S. Aththajariyakul, Development of automobile Bangkok driving cycle for emissions and fuel consumption assessment, The 2nd Joint International Conference on “Sustainable Energy and Environment (SEE 2006)” (2006).
- [21] J.H. Kent, G.H. Allen, G. Rule, A driving cycle for Sydney, *Transp. Res.* 12 (3) (1978) 147–152.
- [22] G.-H. Tzeng, J.-J. Chen, Developing A Taipei motorcycle driving cycle for emissions and fuel economy, *Transportation Research Part D: Transport and Environment* 3 (1) (1998) 19–27.
- [23] H.Y. Tong, W.T. Hung, A framework for developing driving cycles with on-road driving data, *Transp. Rev.* 30 (5) (2010) 589–615.
- [24] R. Smit, J. McBroom, Use of microscopic simulation models to predict traffic emissions, *Road Transp. Res.* 18 (2) (2009) 49–54.
- [25] A. Ravey, et al., Energy-source-Sizing methodology for hybrid fuel cell vehicles based on statistical description of driving cycles, *IEEE Trans. Veh. Technol.* 60 (9) (2011) 4164–4174.
- [26] B.Y. Liaw, M. Dubarry, From driving cycle analysis to understanding battery performance in real-life electric hybrid vehicle operation, *J. Power Sources* 174 (1) (2007) 76–88.
- [27] R. O'Hayre, et al., Introduction, *Fuel Cell Fundamentals*, John Wiley & Sons, Inc., Hoboken, New Jersey, 2016.
- [28] H.S. Das, C.W. Tan, A.H.M. Yatim, Fuel cell hybrid electric vehicles: a review on power conditioning units and topologies, *Renew. Sustain. Energy Rev.* 76 (2017) 268–291.
- [29] UCL Department of Civil Environmental and Geomatic Engineering, Pedestrian Accessibility Movement Environment Laboratory (PAMELA), [cited 2019 7th February]; Available from: (2019) <https://www.ucl.ac.uk/civil-environmental-geomatic-engineering/research/groups-and-centres/pedestrian-accessibility-movement-environment-laboratory-pamela>.
- [30] Department of Transport, Inclusive Mobility, United Kingdom Government, 2005.
- [31] Transport for London, Accessible Bus Stop Design Guidance. For Consultation, Transport for London, 2014.
- [32] L. Beale, et al., Mapping for wheelchair users: route navigation in urban spaces, *Cartogr. J.* 43 (1) (2006) 68–81.
- [33] H. Matthews, et al., Modelling Access with GIS in Urban Systems (MAGUS): capturing the experiences of wheelchair users, *Area* 35 (1) (2003) 34–45.
- [34] C. Holloway, N. Tyler, A micro-level approach to measuring the accessibility of footways for wheelchair users using the Capability Model, *Transp. Plan. Technol.* 36 (7) (2013) 636–649.
- [35] C. Holloway, The Effect of Footway Crossfall Gradient on Wheelchair Accessibility, University College, London, 2011.
- [36] Department of Transport, The Highway Code, United Kingdom Government, 2016.
- [37] T.D. Gillespie, E. Society of Automotive and S.A.E. International (Ed.), Fundamentals of Vehicle Dynamics, SAE International, Warrendale, PA, 1992.
- [38] The energy savings network, U.S. Department of Energy (Ed.), Determining Electric Motor Load Efficiency, 2014.
- [39] Q. Cai, et al., A sizing-design methodology for hybrid fuel cell power systems and its application to an unmanned underwater vehicle, *J. Power Sources* 195 (19) (2010) 6559–6569.
- [40] N. Nitta, et al., Li-ion battery materials: present and future, *Mater. Today* 18 (5) (2015) 252–264.
- [41] Pragma Industries, Metal Hybride Tanks, [cited 2019 7th February]; Available from: https://www.pragma-industries.com/wp-content/themes/default/images/MH_TANKS.pdf.
- [42] C. Auger, et al., Life-space mobility of middle-aged and older adults at various stages of usage of power mobility devices, *Arch. Phys. Med. Rehabil.* 91 (5) (2010) 765–773.
- [43] A. Karmarkar, et al., Evaluation of pushrim-activated power-assisted wheelchairs using ANSI/RESNA standards, *Arch. Phys. Med. Rehabil.* 89 (6) (2008) 1191–1198.
- [44] M.U. Karaođlan, N.S. Kuralay, C.O. Colpan, Investigation of the effects of battery types and power management algorithms on drive cycle simulation for a range-extended electric vehicle powertrain, *Int. J. Green Energy* 16 (1) (2019) 1–11.
- [45] B. Wang, et al., Energy consumption analysis of different bev powertrain topologies by design optimization, *Int. J. Automot. Technol.* 19 (5) (2018) 907–914.
- [46] G. Napoli, et al., Development of a fuel cell hybrid electric powertrain: a real case study on a Minibus application, *Int. J. Hydrogen Energy* 42 (46) (2017) 28034–28047.
- [47] A. Alaswad, et al., Developments in fuel cell technologies in the transport sector, *Int. J. Hydrogen Energy* 41 (37) (2016) 16499–16508.
- [48] D.Z. Morgado Ramirez, et al., Electric Wheelchair Power and Drive Cycle 2016–2017, UK Data Service, Colchester, Essex, 2019 10.5255/UKDA-SN-853486, re-share.ukdataservice.ac.uk/853486.